New Journal of Physics
The open access journal at the forefront of physics

Deutsche Physikalische Gesellschaft DPG IOP Institute of Physics

PAPER • OPEN ACCESS

Topological Weyl semimetals in the chiral antiferromagnetic materials Mn_3Ge and Mn_3Sn

To cite this article: Hao Yang *et al* 2017 *New J. Phys.* **19** 015008

New Journal of Physics
The open access journal at the forefront of physics

Deutsche Physikalische Gesellschaft DPG
IOP Institute of Physics

Published in partnership with: Deutsche Physikalische Gesellschaft and the Institute of Physics

OPEN ACCESS

RECEIVED
10 August 2016

REVISED
15 November 2016

ACCEPTED FOR PUBLICATION
19 December 2016

PUBLISHED
20 January 2017

PAPER

Topological Weyl semimetals in the chiral antiferromagnetic materials Mn_3Ge and Mn_3Sn

Hao Yang[1,2], **Yan Sun**[1], **Yang Zhang**[1,3], **Wu-Jun Shi**[1,4], **Stuart S P Parkin**[2] **and Binghai Yan**[1,5]

[1] Max Planck Institute for Chemical Physics of Solids, D-01187 Dresden, Germany
[2] Max Planck Institute of Microstructure Physics, Weinberg 2, D-06120 Halle, Germany
[3] Leibniz Institute for Solid State and Materials Research, D-01069 Dresden, Germany
[4] School of Physical Science and Technology, ShanghaiTech University, Shanghai 200031, People's Republic of China
[5] Max Planck Institute for the Physics of Complex Systems, D-01187 Dresden, Germany

E-mail: yan@cpfs.mpg.de

Keywords: Weyl semimetal, antiferromagnetism, anomalous Hall effect, surface states, Fermi arcs

Abstract

Recent experiments revealed that Mn_3Sn and Mn_3Ge exhibit a strong anomalous Hall effect at room temperature, provoking us to explore their electronic structures for topological properties. By *ab initio* band structure calculations, we have observed the existence of multiple Weyl points in the bulk and corresponding Fermi arcs on the surface, predicting antiferromagnetic Weyl semimetals in Mn_3Ge and Mn_3Sn. Here the chiral antiferromagnetism in the Kagome-type lattice structure is essential to determine the positions and numbers of Weyl points. Our work further reveals a new guiding principle to search for magnetic Weyl semimetals among materials that exhibit a strong anomalous Hall effect.

1. Introduction

Recent discovery of Weyl semimetals (WSMs) [1–3] in realistic materials has stimulated tremendous research interest in topological semimetals, such as WSMs, Dirac semimetals, and nodal line semimetals [4–9], as a new frontier of condensed matter physics after the discovery of topological insulators [10, 11]. The WSMs are of particular interest not only because of their exotic Fermi-arc-type surface states but also because of their appealing bulk chiral magneto-transport properties, such as the chiral anomaly effect [12–14], nonlocal transport [15, 16], large magnetoresistance, and high mobility [17]. Currently discovered WSM materials can be classified into two groups. One group breaks crystal inversion symmetry but preserves time-reversal symmetry (e.g., TaAs-family transition-metal pnictides [18, 19] and WTe_2- and $MoTe_2$-family transition-metal dichalcogenides [20–26]). The other group breaks time-reversal symmetry in ferromagnets with possible tilted moments (e.g., magnetic Heusler GdPtBi [27, 28] and $YbMnBi_2$ [29]). An antiferromagnetic (AFM) WSM compound has yet to be found, although $Y_2Ir_2O_7$ with a noncoplanar AFM structure was theoretically predicted to be a WSM candidate [5].

In a WSM, the conduction and valence bands cross each other linearly through nodes called Weyl points. Between a pair of Weyl points with opposite chiralities (sink or source of the Berry curvature) [4], the emerging Berry flux can lead to the anomalous Hall effect (AHE) [30], as observed in GdPtBi [27, 28], and an intrinsic spin Hall effect (SHE), as predicted in TaAs-type materials [31], for systems without and with time-reversal symmetry, respectively. Herein, we raise a simple recipe to search for WSM candidates among materials that host strong AHE or SHE.

Recently, Mn_3X (where X = Sn, Ge, and Ir), which exhibit noncollinear antiferromagetic (AFM) phases at room temperature, have been found to show large AHE [32–35] and SHE [36], provoking our interest to investigate their band structures for possible WSMs. In this work, we report the existence of Weyl fermions for Mn_3Ge and Mn_3Sn compounds and the resultant Fermi arcs on the surface by *ab initio* calculations, awaiting experimental verifications. Dozens of Weyl points exist near the Fermi energy in their band structure, and these can be well understood with the assistance of lattice symmetry.

2. Methods

The electronic ground states of Mn_3Ge and Mn_3Sn were calculated by using density-functional theory (DFT) within the Perdew–Burke–Ernzerhof-type generalized-gradient approximation (GGA) [37] using the Vienna *ab initio* simulation package (VASP) [38]. The $3d^64s^1$, $4s^24p^2$, and $5s^25p^2$ electrons were considered as valance electrons for Mn, Ge, and Sn atoms, respectively. The primitive cell with experimental crystal parameters $a = b = 5.352$ and $c = 4.312$ Å for Mn_3Ge and $a = b = 5.67$ and $c = 4.53$ Å for Mn_3Sn were adopted. Spin-orbit coupling (SOC) was included in all calculations.

To identify the Weyl points with the monopole feature, we calculated the Berry curvature distribution in momentum space. The Berry curvature was calculated based on a tight-binding Hamiltonian based on localized Wannier functions [39] projected from the DFT Bloch wave functions. Chosen were atomic-orbital-like Wannier functions, which include Mn-spd and Ge-sp/Sn-p orbitals, so that the tight-binding Hamiltonian is consistent with the symmetry of *ab initio* calculations. From such a Hamiltonian, the Berry curvature can be calculated using the Kubo-formula approach [40]

$$\Omega_n^{\gamma}(\vec{k}) = 2i\hbar^2 \sum_{m \neq n} \frac{\langle u_n(\vec{k})|\hat{v}_{\alpha}|u_m(\vec{k})\rangle \langle u_m(\vec{k})|\hat{v}_{\beta}|u_n(\vec{k})\rangle}{(E_n(\vec{k}) - E_m(\vec{k}))^2}, \quad (1)$$

where $\Omega_n^{\gamma}(\vec{k})$ is the Berry curvature in momentum space for a given band n, $\hat{v}_{\alpha(\beta,\gamma)} = \frac{1}{\hbar}\frac{\partial \hat{H}}{\partial k_{\alpha(\beta,\gamma)}}$ is the velocity operator with $\alpha, \beta, \gamma = x, y, z$, and $|u_n(\vec{k})\rangle$ and $E_n(\vec{k})$ are the eigenvector and eigenvalue of the Hamiltonian $\hat{H}(\vec{k})$, respectively. The summation of $\Omega_n^{\gamma}(\vec{k})$ over all valence bands gives the Berry curvature vector $\mathbf{\Omega}$ (Ω^x, Ω^y, Ω^z).

In addition, the surface states that demonstrate the Fermi arcs were calculated on a semi-infinite surface, where the momentum-resolved local density of states (LDOS) on the surface layer was evaluated based on the Green's function method. We note that the current surface band structure corresponds to the bottom surface of a half-infinite system.

3. Results and discussion

3.1. Symmetry analysis of the AFM structure

Mn_3Ge and Mn_3Sn share the same layered hexagonal lattice (space group $P6_3/mmc$, No. 194). Inside a layer, Mn atoms form a Kagome-type lattice with mixed triangles and hexagons and Ge/Sn atoms are located at the centers of these hexagons. Each Mn atom carries a magnetic moment of 3.2 μB in Mn_3Sn and 2.7 μB in Mn_3Ge. As revealed in a previous study [41], the ground magnetic state is a noncollinear AFM state, where Mn moments align inside the *ab* plane and form 120° angles with neighboring moment vectors, as shown in figure 1(b). Along the *c* axis, stacking two layers leads to the primitive unit cell. Given the magnetic lattice, these two layers can be transformed into each other by inversion symmetry or with a mirror reflection (M_y) adding a half-lattice ($c/2$) translation, i.e., a nonsymmorphic symmetry $\{M_y|\tau = c/2\}$. In addition, two other mirror reflections (M_x and M_z) adding time reversal (T), M_xT and M_zT, exist.

In momentum space, we can utilize three important symmetries, M_xT, M_zT, and M_y, to understand the electronic structure and locate the Weyl points. Suppose a Weyl point with chirality χ (+ or −) exists at a generic position $\mathbf{k}$ (k_x, k_y, k_z). Mirror reflection reverses χ while time reversal does not and both of them act on $\mathbf{k}$. Further, mirror reflection M_γ preserves the Berry curvature Ω^γ while time reversal reserves it. The transformation is as follows:

$$\begin{aligned} M_xT &: (k_x, k_y, k_z) \to (k_x, -k_y, -k_z);\ \chi \to -\chi;\ \Omega^x \to -\Omega^x \\ M_zT &: (k_x, k_y, k_z) \to (-k_x, -k_y, k_z);\ \chi \to -\chi;\ \Omega^z \to -\Omega^z \\ M_y &: (k_x, k_y, k_z) \to (k_x, -k_y, k_z);\ \chi \to -\chi;\ \Omega^y \to +\Omega^y. \end{aligned} \quad (2)$$

Each of the above three operations doubles the number of Weyl points. Thus, eight nonequivalent Weyl points can be generated at $(\pm k_x, +k_y, \pm k_z)$ with chirality χ and $(\pm k_x, -k_y, \pm k_z)$ with chirality $-\chi$ (see figure 1(c)). We note that the $k_x = 0/\pi$ or $k_z = 0/\pi$ plane can host Weyl points. However, the $k_y = 0/\pi$ plane cannot host Weyl points, because M_y simply reverses the chirality and annihilates the Weyl point with its mirror image if it exists.

In addition, the symmetry of the 120° AFM state is slightly broken in the materials, owing to the existence of a tiny net moment (~0.003 μB per unit cell) [41–43]. Such weak symmetry breaking seems to induce negligible effects in the transport measurement. However, it gives rise to a perturbation of the band structure, for example, shifting slightly the mirror image of a Weyl point from its position expected, as we will see in the surface states of Mn_3Ge.

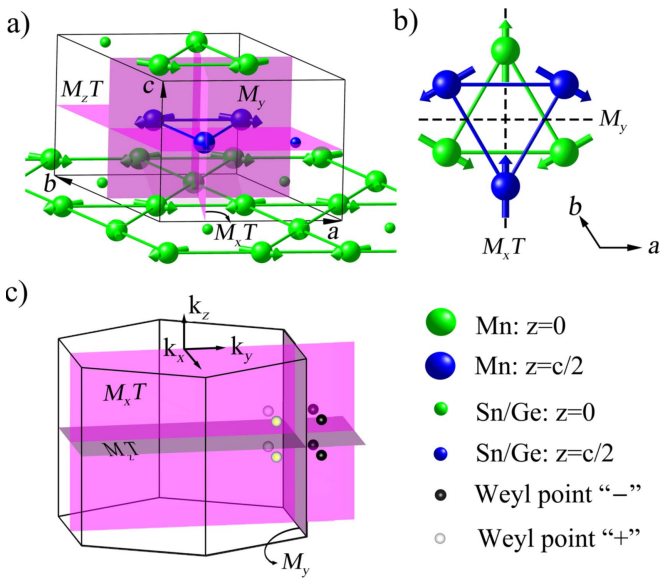

Figure 1. Crystal and magnetic structures of Mn_3X (where X = Sn or Ge) and related symmetry. (a) Crystal structure of Mn_3X. Three mirror planes are shown in purple, corresponding to $\{M_y|\tau = c/2\}$, M_xT, and M_zT symmetries. (b) Top view along the c axis of the Mn sublattice. Chiral AFM with an angle of 120° between neighboring magnetic moments is formed in each Mn layer. The mirror planes that correspond to M_xT and $\{M_y|\tau = c/2\}$ are marked by dashed lines. (c) Symmetry in momentum space, M_y, M_xT, and M_zT. If a Weyl point appears at (k_x, k_y, k_z), eight Weyl points in total can be generated at $(\pm k_x, \pm k_y, \pm k_z)$ by the above three symmetry operations. For convenience, we choose the $k_y = \pi$ plane for M_y here.

3.2. The anomalous Hall effect

The intrinsic anomalous Hall conductivity σ_γ ($\gamma = x, y, z$) can be calculated by integrating the Berry curvature Ω^γ over the whole Brillouin zone [40, 44]

$$\sigma^\gamma = -\frac{e^2}{\hbar}\int_{BZ}\frac{\mathrm{d}^3\vec{k}}{(2\pi)^3}f_n(\vec{k})\Omega^\gamma(\vec{k}). \tag{3}$$

According to equation (2), Ω^x and Ω^z are odd with respect to $M_x T$ and $M_y T$, respectively. Thus, corresponding σ^x and σ^z are zero. Since Ω^y is even with respect to the M_y mirror plane, corresponding σ^y is nonzero. This is also consistent with the distribution of Weyl points in the k-space. As shown in figure 1(c), only '+' Weyl points appear on one side of the M_y plane and only '–' Weyl points locate on the other side of M_y plane. Then there are net Berry flux (starting from '+' to '–' Weyl points) Ω^y crossing the M_y plane, resulting in the nonzero anomalous Hall conductivity σ^y. In contrast, an equal number of '+' and '–' Weyl points appear on each side of M_x (M_z) planes. Consequently, the net Berry flux of Ω^x (Ω^z) should be zero, giving rise to vanishing σ^x (σ^z). According to recent numerical calculations [36], σ^y = 330(133) S^{-1} cm^{-1} for Mn_3Ge (Mn_3Sn).

In the measurement of AHE, an external magnetic field is usually applied to uniform different magnetic domains. Further, for Mn_3Ge and Mn_3Sn, the triangular spins can be rotated inside the xy plane even by a very weak magnetic field due to the residual magnetic moment [43]. The rotation of an arbitrary angle can break the M_y and $M_x T$ symmetry, showing nonzero σ^y and σ^x. However, σ^z is still zero due to the $M_z T$ symmetry. As observed for both compounds in experiment [34, 35], $\sigma^{x,y}$ are indeed very large and σ^z is negligible. The in-plane anomalous Hall conductivity is about 500 (100) S^{-1} cm^{-1} for Mn_3Ge (Mn_3Sn) at low temperature, which are in the same order of magnitude as the calculations [36].

3.3. Weyl points in the bulk band structure

The bulk band structures are shown along high-symmetry lines in figure 2 for Mn_3Ge and Mn_3Sn. It is not surprising that the two materials exhibit similar band dispersions. At first glance, one can find two seemingly band degenerate points at Z and K points, which are below the Fermi energy. Because of $M_z T$ and the nonsymmorphic symmetry $\{M_y|\tau = c/2\}$, the bands are supposed to be quadruply degenerate at the Brillouin zone boundary Z, forming a Dirac point protected by the nonsymmorphic space group [45–47]. Given the slight mirror symmetry breaking by the residual net magnetic moment, this Dirac point is gapped at Z (as shown in the enlarged panel) and splits into four Weyl points, which are very close to each other in k space. A tiny gap also appears at the K point. Nearby, two additional Weyl points appear, too. Since the Weyl point separations are too small near both Z and K points, these Weyl points may generate little observable consequence in experiments such as those for studying Fermi arcs. Therefore, we will not focus on them in the following investigation.

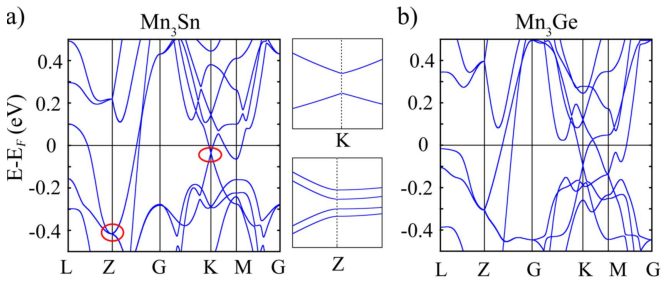

Figure 2. Bulk band structures for (a) Mn_3Sn and (b) Mn_3Ge along high-symmetry lines with SOC. The bands near the Z and K (indicated by red circles) are expanded to show details in (a). The Fermi energy is set to zero.

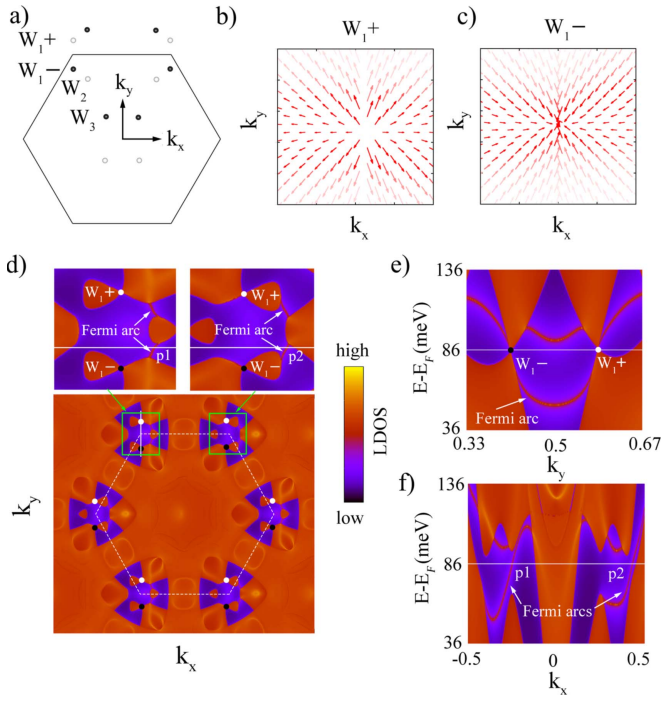

Figure 3. Surface states of Mn_3Sn. (a) Distribution of Weyl points in momentum space. Black and white points represent Weyl points with − and + chirality, respectively. (b) and (c) monopole-like distribution of the Berry curvature near a W_1 Weyl point. (d) Fermi surface at $E_F = 86$ meV crossing the W_1 Weyl points. The color represents the surface LDOS. Two pairs of W_1 points are shown enlarged in the upper panels, where clear Fermi arcs exist. (e) Surface band structure along a line connecting a pair of W_1 points with opposite chirality. (f) Surface band structure along the white horizontal line indicated in (d). Here p1 and p2 are the chiral states corresponding to the Fermi arcs.

Mn_3Sn and Mn_3Ge are actually metallic, as seen from the band structures. However, we retain the terminology of Weyl semimetal for simplicity and consistency. The valence and conduction bands cross each many times near the Fermi energy, generating multiple pairs of Weyl points. We first investigate the Sn compound. Supposing that the total valence electron number is N_v, we search for the crossing points between the N_v^{th} and $(N_v + 1)^{th}$ bands.

As shown in figure 3(a), there are six pairs of Weyl points in the first Brillouin zone; these can be classified into three groups according to their positions, noted as W_1, W_2, and W_3. These Weyl points lie in the M_z plane (with W_2 points being only slightly off this plane owing to the residual-moment-induced symmetry breaking) and slightly above the Fermi energy. Therefore, there are four copies for each of them according to the symmetry analysis in equation (2). Their representative coordinates and energies are listed in table 1 and also indicated in figure 3(a). A Weyl point (e.g., W_1 in figures 3(b) and (c)) acts as a source or sink of the Berry curvature $\boldsymbol{\Omega}$, clearly showing the monopole feature with a definite chirality.

In contrast to Mn_3Sn, Mn_3Ge displays many more Weyl points. As shown in figure 4(a) and listed in table 2, there are nine groups of Weyl points. Here $W_{1,2,7,9}$ lie in the M_z plane with W_9 on the k_y axis, W_4 appears in the M_x plane, and the others are in generic positions. Therefore, there are four copies of $W_{1,2,7,4}$, two copies of W_9, and eight copies of other Weyl points. Although there are many other Weyl points in higher energies owing to

Table 1. Positions and energies of Weyl points in first Brillouin zone for Mn_3Sn. The positions (k_x, k_y, k_z) are in units of π. Energies are relative to the Fermi energy E_F. Each type of Weyl point has four copies whose coordinates can be generated from the symmetry as ($\pm k_x$, $\pm k_y$, $k_z = 0$).

Weyl point	k_x	k_y	k_z	Chirality	Energy (meV)
W_1	−0.325	0.405	0.000	−	86
W_2	−0.230	0.356	0.003	+	158
W_3	−0.107	0.133	0.000	−	493

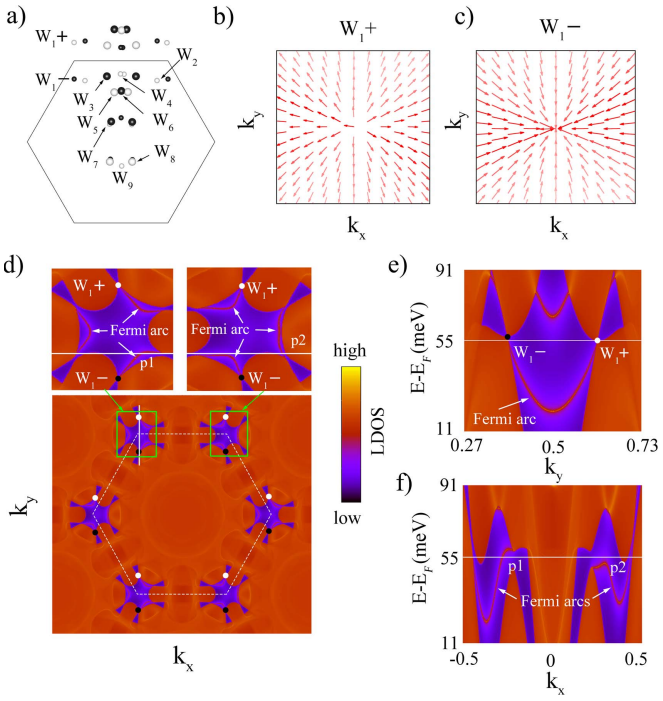

Figure 4. Surface states of Mn_3Ge. (a) Distribution of Weyl points in momentum space. Black and white points represent Weyl points with − and + chirality, respectively. Larger points indicate two Weyl points ($\pm k_z$) projected into this plane. (b) and (c) monopole-like distribution of the Berry curvature near a W_1 Weyl point. (d) Fermi surface at $E_F = 55$ meV crossing the W_1 Weyl points. The color represents the surface LDOS. Two pairs of W_1 points are shown enlarged in the upper panels, where clear Fermi arcs exist. (e) Surface band structure along a line connecting a pair of W_1 points with opposite chirality. (f) Surface band structure along the white horizontal line indicated in (d). Here p1 and p2 are the chiral states corresponding to the Fermi arcs.

Table 2. Positions and energies of Weyl points in the first Brillouin zone for Mn_3Ge. The positions (k_x, k_y, k_z) are in units of π. Energies are relative to the Fermi energy E_F. Each of $W_{1,2,7}$ has four copies whose coordinates can be generated from the symmetry as ($\pm k_x$, $\pm k_y$, $k_z = 0$). W_4 has four copies at ($k_x \approx 0$, $\pm k_y$, $\pm k_z$) and W_9 has two copies at ($k_x \approx 0$, $\pm k_y$, $k_z = 0$). Each of the other Weyl points has four copies whose coordinates can be generated from the symmetry as ($\pm k_x$, $\pm k_y$, $\pm k_z$).

Weyl point	k_x	k_y	k_z	Chirality	Energy (meV)
W_1	−0.333	0.388	−0.000	−	57
W_2	0.255	0.378	−0.000	+	111
W_3	−0.101	0.405	0.097	−	48
W_4	−0.004	0.419	0.131	+	8
W_5	−0.048	0.306	0.164	+	77
W_6	0.002	0.314	0.171	−	59
W_7	−0.081	0.109	0.000	+	479
W_8	0.069	−0.128	0.117	+	330
W_9	0.004	−0.149	−0.000	+	470

different band crossings, we mainly focus on the current Weyl points that are close to the Fermi energy. The monopole-like distribution of the Berry curvature near these Weyl points is verified; see W_1 in figure 4 as an example. Without including SOC, we observed a nodal-ring-like band crossing in the band structures of both Mn_3Sn and Mn_3Ge. SOC gaps the nodal rings but leaves isolating band-touching points, i.e., Weyl points. Since Mn_3Sn exhibits stronger SOC than Mn_3Ge, many Weyl points with opposite chirality may annihilate each other by being pushed by the strong SOC in Mn_3Sn. This might be why Mn_3Sn exhibits fewer Weyl points than Mn_3Ge.

3.4. Fermi arcs on the surface

The existence of Fermi arcs on the surface is one of the most significant consequences of Weyl points inside the three-dimensional (3D) bulk. We first investigate the surface states of Mn_3Sn that have a simple bulk band structure with fewer Weyl points. When projecting $W_{2,3}$ Weyl points to the (001) surface, they overlap with other bulk bands that overwhelm the surface states. Luckily, W_1 Weyl points are visible on the Fermi surface. When the Fermi energy crosses them, W_1 Weyl points appear as the touching points of neighboring hole and electron pockets. Therefore, they are typical type-II Weyl points [20, 48]. Indeed, their energy dispersions demonstrate strongly tilted Weyl cones.

The Fermi surface of the surface band structure is shown in figure 3(d) for the Sn compound. In each corner of the surface Brillouin zone, a pair of W_1 Weyl points exists with opposite chirality. Connecting such a pair of Weyl points, a long Fermi arc appears in both the Fermi surface (figure 3(d) and the band structure (figure 3(e)). Although the projection of bulk bands exhibit pseudo-symmetry of a hexagonal lattice, the surface Fermi arcs do not. It is clear that the Fermi arcs originating from two neighboring Weyl pairs (see figure 3(d)) do not exhibit M_x reflection, because the chirality of Weyl points apparently violates M_x symmetry. For a generic k_x–k_z plane between each pair of W_1 Weyl points, the net Berry flux points in the $-k_y$ direction. As a consequence, the Fermi velocities of both Fermi arcs point in the $+k_x$ direction on the bottom surface (see figure 3(f)). These two right movers coincide with the nonzero net Berry flux, i.e., Chern number $= 2$.

For Mn_3Ge, we also focus on the W_1-type Weyl points at the corners of the hexagonal Brillouin zone. In contrast to Mn_3Sn, Mn_3Ge exhibits a more complicated Fermi surface. Fermi arcs exist to connect a pair of W_1-type Weyl points with opposite chirality, but they are divided into three pieces as shown in figure 4(d). In the band structures (see figures 4(e) and (f)), these three pieces are indeed connected together as a single surface state. Crossing a line between two pairs of W_1 points, one can find two right movers in the band structure, which are indicated as p1 and p2 in figure 4(f). The existence of two chiral surface bands is consistent with a nontrivial Chern number between these two pairs of Weyl points.

4. Summary

In summary, we have discovered the Weyl semimetal state in the chiral AFM compounds Mn_3Sn and Mn_3Ge by *ab initio* band structure calculations. Multiple Weyl points were observed in the bulk band structures, most of which are type II. The positions and chirality of Weyl points are in accordance with the symmetry of the magnetic lattice. For both compounds, Fermi arcs were found on the surface, each of which connects a pair of Weyl points with opposite chirality, calling for further experimental investigations such as angle-resolved photoemission spectroscopy. The discovery of Weyl points verifies the large anomalous Hall conductivity observed recently in titled compounds. Our work further reveals a guiding principle to search for Weyl semimetals among materials that exhibit a strong anomalous Hall effect.

Acknowledgments

We thank Claudia Felser, Jürgen Kübler and Ajaya K Nayak for helpful discussions. We acknowledge the Max Planck Computing and Data Facility (MPCDF) and Shanghai Supercomputer Center for computational resources and the German Research Foundation (DFG) SFB-1143 for financial support.

References

[1] Lv B Q *et al* 2015 *Phys. Rev.* X **5** 031013
[2] Xu S-Y *et al* 2015 *Science* **349** 613
[3] Yang L X *et al* 2015 *Nat. Phys.* **11** 728
[4] Volovik G E 2003 *The Universe in a Helium Droplet* (Oxford: Clarendon)
[5] Wan X G, Turner A M, Vishwanath A and Savrasov S Y 2011 *Phys. Rev.* B **83** 205101
[6] Balents L 2011 *Physics* **4** 36
[7] Burkov A A, Hook M D and Balents L 2011 *Phys. Rev.* B **84** 235126

[8] Hosur P and Qi X L 2013 *C. R. Phys.* **14** 857
[9] Vafek O and Vishwanath A 2014 *Annu. Rev. Condens. Matter Phys.* **5** 83
[10] Qi X-L and Zhang S-C 2011 *Rev. Mod. Phys.* **83** 1057
[11] Hasan M Z and Kane C L 2010 *Rev. Mod. Phys.* **82** 3045
[12] Xiong J, Kushwaha S K, Liang T, Krizan J W, Hirschberger M, Wang W, Cava R J and Ong N P 2015 *Science* **350** 413
[13] Huang X *et al* 2015 *Phys. Rev.* X **5** 031023
[14] Arnold F *et al* 2016 *Nat. Commun.* **7** 11615
[15] Parameswaran S, Grover T, Abanin D, Pesin D and Vishwanath A 2014 *Phys. Rev.* X **4** 031035
[16] Baum Y, Berg E, Parameswaran S A and Stern A 2015 *Phys. Rev.* X **5** 041046
[17] Shekhar C *et al* 2015 *Nat. Phys.* **11** 645
[18] Weng H, Fang C, Fang Z, Bernevig B A and Dai X 2015 *Phys. Rev.* X **5** 011029
[19] Huang S-M *et al* 2015 *Nat. Commun.* **6** 8373
[20] Soluyanov A A, Gresch D, Wang Z, Wu Q, Troyer M, Dai X and Bernevig B A 2015 *Nature* **527** 495
[21] Sun Y, Wu S C, Ali M N, Felser C and Yan B 2015 *Phys. Rev.* B **92** 161107R
[22] Wang Z, Gresch D, Soluyanov A A, Xie W, Kushwaha S, Dai X, Troyer M, Cava R J and Bernevig B A 2016 *Phys. Rev. Lett.* **117** 056805
[23] Koepernik K, Kasinathan D, Efremov D V, Khim S, Borisenko S, Büchner B and van den Brink J 2016 *Phys. Rev.* B **93** 201101
[24] Deng K *et al* 2016 *Nat. Phys.* **12** 1105-10
[25] Jiang J *et al* 2016 arXiv:1604.00139
[26] Tamai A *et al* 2016 *Phys. Rev.* X **6** 031021
[27] Hirschberger M, Kushwaha S, Wang Z, Gibson Q, Liang S, Belvin C A, Bernevig B A, Cava R J and Ong N P 2016 *Nat. Mater.* **15** 1161
[28] Shekhar C, Nayak A K, Singh S and Kumar N 2016 arXiv:1604.01641
[29] Borisenko S, Evtushinsky D, Gibson Q, Yaresko A, Kim T, Ali M N, Buechner B, Hoesch M and Cava R J 2015 arXiv:1507.04847
[30] Burkov A A 2014 *Phys. Rev. Lett.* **113** 187202
[31] Sun Y, Zhang Y, Felser C and Yan B 2016 *Phys. Rev. Lett.* **117** 146403
[32] Kübler J and Felser C 2014 *Europhys. Lett.* **108** 67001
[33] Chen H, Niu Q and MacDonald A H 2014 *Phys. Rev. Lett.* **112** 017205
[34] Nakatsuji S, Kiyohara N and Higo T 2015 *Nature* **527** 212
[35] Nayak A K *et al* 2016 *Sci. Adv.* **2** e1501870
[36] Zhang W, Han W, Yang S H, Sun Y, Zhang Y, Yan B and Parkin S 2016 *Sci. Adv.* **2** e1600759
[37] Perdew J P, Burke K and Ernzerhof M 1996 *Phys. Rev. Lett.* **77** 3865
[38] Kresse G and Furthmüller J 1996 *Comput. Mater. Sci.* **6** 15
[39] Mostofi A A, Yates J R, Lee Y-S, Souza I, Vanderbilt D and Marzari N 2008 *Comput. Phys. Commun.* **178** 685
[40] Xiao D, Chang M-C and Niu Q 2010 *Rev. Mod. Phys.* **82** 1959
[41] Zhang D, Yan B, Wu S-C, Kübler J, Kreiner G, Parkin S S and Felser C 2013 *J. Phys.: Condens. Matter* **25** 206006
[42] Nagamiya T, Tomiyoshi S and Yamaguchi Y 1982 *Solid State Commun.* **42** 385
[43] Tomiyoshi S and Yamaguchi Y 1982 *J. Phys. Soc. Japan* **51** 2478
[44] Nagaosa N, Sinova J, Onoda S, MacDonald A H and Ong N P 2010 *Rev. Mod. Phys.* **82** 1539
[45] Young S M, Zaheer S, Teo J C Y, Kane C L, Mele E J and Rappe A M 2012 *Phys. Rev. Lett.* **108** 140405
[46] Schoop L M, Ali M N, Straßer C, Topp A, Varykhalov A, Marchenko D, Duppel V, Parkin S S P, Lotsch B V and Ast C R 2000 *Nat. Commun.* **7** 11696
[47] Tang P, Zhou Q, Xu G and Zhang S-C 2016 *Nat. Phys.* **12** 1100–4
[48] Yong X, Fan Z and Chuanwei Z 2015 *Phys. Rev. Lett.* **115** 265304